Tidal meanders

Marco Marani, Stefano Lanzoni, and Diego Zandolin
Dipartimento Ingegneria Idraulica, Marittima e Geotecnica, Universitá di Padova, Padova, Italy

Giovanni Seminara
Dipartimento Ingegneria Ambientale, Universitá di Genova, Genova, Italy

Andrea Rinaldo
Dipartimento Ingegneria Idraulica, Marittima e Geotecnica, Universitá di Padova, Padova, Italy

Received 13 February 2001; revised 12 February 2002; accepted 12 February 2002; published 8 November 2002.

[1] Observational evidence is presented on the geometry of meandering tidal channels evolved within coastal wetlands characterized by different tidal, hydrodynamic, topographic, vegetational and ecological features. New insight is provided on the geometrical properties of tidal meanders, with possible dynamic implications on their evolution. In particular, it is shown that large spatial gradients of leading flow rates induce important spatial variabilities of meander wavelengths and widths, while their ratio remains remarkably constant in the range of scales of observation. This holds regardless of changes in width and wavelength up to two orders of magnitude. This suggests a locally adapted evolution, involving the morphological adjustment to the chief landforming events driven by local hydrodynamics. The spectral analysis of local curvatures reveals that Kinoshita's model curve does not fit tidal meanders due to the presence of even harmonics, in particular the second mode. Geometric parameters are constructed that are suitable to detect possible geomorphic signatures of the transitions from ebb- to flood-dominated hydrodynamics, here related to the skewness of the tidal meander. Trends in skewness, however, prove elusive to measure and fail to show detectable patterns. We also study comparatively the spatial patterns of evolution of the ratios of channel width to depth, and the ratio of width to local radius of curvature. Interestingly, the latter ratio exhibits consistency despite sharp differences in channel incision. Since the degree of incision, epitomized by the width-to-depth ratio, responds to the relevant erosion and migrations mechanisms and is much sensitive to vegetation and sediment properties, it is noticeable that we observe a great variety of landscape carving modes and yet recurrent planar features like constant width/curvature and wavelength/width ratios. *INDEX TERMS:* 1824 Hydrology: Geomorphology (1625); 1815 Hydrology: Erosion and sedimentation; 4235 Oceanography: General: Estuarine processes; *KEYWORDS:* meanders, tidal channels, morphodynamics

Citation: Marani, M., S. Lanzoni, D. Zandolin, G. Seminara, and A. Rinaldo, Tidal meanders, *Water Resour. Res.*, *38*(11), 1225, doi:10.1029/2001WR000404, 2002.

1. Introduction

[2] Coastal wetlands exist in a state, seldom in dynamic equilibrium, balancing strong counteracting forces (both acting in the horizontal and vertical planes) leading either to their establishment and maintenance or to their deterioration [e.g., *Day et al.*, 1999]. Chief landforming processes in the vertical plane are the combined actions of subsidence and sea level rise possibly compensated by accretion processes. The resulting balance is complex and affected by many factors of physical, chemical and biological nature. Accretion rates are possibly offset by the rates of sea level rise [*Day et al.*, 1999], but often self-tuned in nature to balance it and thus leading to the survival of the tidal landforms for long periods of time [*Redfield*, 1972; *Orson et al.*, 1987]. In the horizontal plane, the development of drainage patterns on tidal marshes, whether ebb- or flood-dominated, controls the hydrodynamics and sediment exchanges between saltmarshes and tidal flats and, in general, within the entire coastal wetland [e.g., *Pestrong*, 1965; *Boon*, 1975; *Pethick*, 1980; *Boon and Byrne*, 1981; *Speer and Aubrey*, 1985; *Friedrichs and Madsen*, 1992; *Friedichs and Aubrey*, 1988; *Friedichs*, 1995; *Steel and Pye*, 1997; *Fagherazzi et al.*, 1999a, 1999b; *Rinaldo et al.*, 1999a, 1999b].

[3] The importance of the careful observation of planar patterns of tidal wetlands, and of the embedded landforms, is linked to the implications on the origin and long-term evolution of the complex of morphological structures which characterize such environments, such as lagoons, deltas or estuaries. A new procedure for the large-scale automatic extraction of the morphological features of the tidal patterns

0043-1397/02/2001WR000404$09.00

from topographic data of channel marsh and tidal flat lands recently allowed a comparative analysis of tidal and fluvial network morphologies, including watershed delineation, scaling features (or lack of them thereof), and geomorphic relationships with landscape-forming flow rates [*Fagherazzi et al.*, 1999a; *Rinaldo et al.*, 1999a, 1999b]. Several morphometric analyses have thus been performed on the structure of the network, in particular to establish the clear departures from fluvial facies. It became apparent, however, that several features of the tidal channels, chiefly the width and the sinuosity of the axis, show strong variations in space unusual in fluvial morphology even over length scales of hundreds to thousands of widths. In any real case of fluvial versus tidal patterns, differences are the norm rather than the exception once carefully examined. In fact, the conclusion of *Fagherazzi et al.* [1999a] is that tidal networks, differently from fluvial counterparts, basically are not scaling structures. This observation bears interesting implications on the relevant physics and on the emergence of self-organized critical patterns in nature (see, for a review of related issues, *Rodriguez-Iturbe and Rinaldo* [1997]) because it had been argued that basically all networks are 'inevitably' invariant across scales, a statement one cannot agree upon. On the contrary, the lack of inevitability in the emergence of scaling properties seems more interesting from a dynamical viewpoint. From this we gather the relevance of the study of tidal patterns, a subject first tackled in this paper by a wide screening of geometric features observed in nature.

[4] Other geomorphic issues of interest in this context concern the possible natural emergence of loops in the network patterns. Whether tree-like (where any point has a unique route to the outlet) or looping patterns are present in the morphology of a tidal network, the observational features, seen as possible stationary states of their evolution, suggest constraints of the relevant morphodynamics [*Banavar et al.*, 2000].

[5] This paper introduces a set of mathematical tools for the objective, automatic analysis of tidal meanders. This proves a rather demanding task, in particular in order to quantitatively characterize the channel morphology where widths are much larger than the size of the elementary representative unit of topographical information (i.e., a pixel of a digital map). This is pursued by establishing links to recent methods and models exploiting digital terrain maps [*Rodriguez-Iturbe and Rinaldo*, 1997; *Fagherazzi et al.*, 1999a]. This approach has also the advantage of enabling objective comparisons of patterns obtained in tidal and fluvial environments [e.g., *Kinoshita*, 1961; *Leopold et al.*, 1964; *Ikeda et al.*, 1981; *Parker et al.*, 1982; *Blondeaux and Seminara*, 1985; *Howard*, 1992, 1996; *Solari et al.*, 2002; *Seminara et al.*, 2001] giving, by contrast or analogy, information on the chief landforming processes shaping the tidal landscapes.

[6] The observations of the geometry of tidal networks on which the present work is based are obtained mainly from the digitalization of aerial photographs or published data and regards tidal environments with different morphological and tidal characteristics. The study areas are the lagoon of Venice (Italy), Petaluma Bay (CA, USA) and Barnstable marsh (MA, USA). For a detailed description of the environments considered and of the processing tools on remote images and on digital terrain maps see *Fagherazzi et al.* [1999a, 1999b] and *Rinaldo et al.* [1999a, 1999b].

2. Morphological Analysis of Tidal Meanders

[7] A first step toward an objective and quantitative characterization of the geometry of tidal channels, requires the classification of each pixel, i.e., elementary area units, within the domain under study. Specifically, one needs to sort whether the arbitrary pixel belongs to channelized regions (the planar pattern of incised regions) and to distinguish it from unchannelized ones in a rasterized representation of the system. Such classification, which proves rather subtle at times owing to the nature of tidal wetlands, may be obtained: (1) automatically from topography through the screening of topographic curvatures [*Fagherazzi et al.*, 1999a]; (2) manually, from aerial photographs and maps [e.g., *Pestrong*, 1965; *Boon*, 1975; *Pethick*, 1980; *Boon and Byrne*, 1981; *Speer and Aubrey*, 1985], or (3) through suitable algorithms applied to remotely sensed data [e.g., *Saccardo*, 1999; *Lohani and Mason*, 1999].

[8] The outcome of the classification procedure, whose details are reported in the literature cited, is a set of channelized pixels outlining the planar pattern of tidal channels. A sample of the observational patterns obtained is shown in Figure 1, where the planar configuration of some of the channels studied, extracted from the three different environments considered, is shown to scale. This rasterized representations constitute the objective basis of the analyses performed in this paper.

[9] In order to analyze the geometries defined by data such as those of Figure 1, it is necessary to use a suitable representation of the channel axis (and/or of border sites when needed). A natural choice of curvilinear coordinate system [e.g., *Leopold and Wolman*, 1957] is based on a mathematical definition of the curve $\Gamma(s) = \{(x(s), y(s)\}$, where x and y are the cartesian coordinates of the arbitrary axis point and s is its intrinsic coordinate (Figure 2). Such a representation avoids problems of uniqueness in the functional relationship $y = f(x)$, which have been argued to have affected previous analyses [e.g., *Sinnock and Rao*, 1984].

[10] A tidal channel, and its meanders, may be described in terms of a number of geometrical properties like radii of curvatures, intrinsic angles or widths, as shown in the Figure 2. In particular, the geometry of the channel axis may be defined through its planar curvature $c(s)$, ($[L^{-1}]$), i.e., the inverse of the local radius of curvature, characterized, as usual, as a function of the intrinsic coordinate s to track its planar development (note that s is assumed to be positive if directed toward the narrower reaches of the channels, i.e, landwards). Important characteristics of a meander are also (1) its intrinsic wavelength, L_s, computed along the s coordinate; and (2) the cartesian wavelength, L_x, defined by the (cartesian) distance between the initial and the end sections of the meander. These sections are located through the inflection points of the axis, i.e., sites s_i where $c(s_i) = 0$, and a meander may be defined as any portion of the channel along s containing three such inflection points. This definition is conceptually reasonable and leads to a relatively simple automatic procedure for delimiting mean-

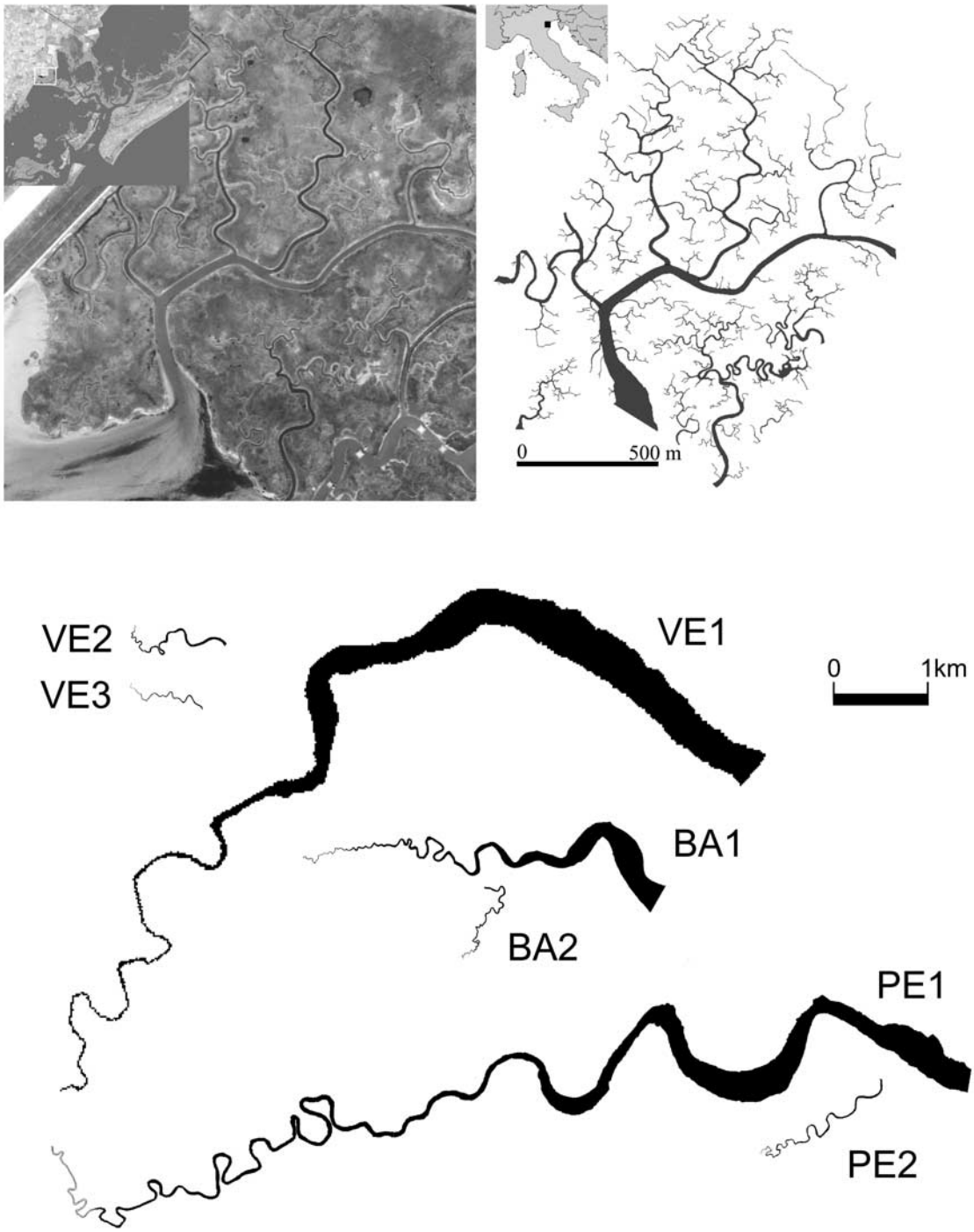

Figure 1. A sample of the database employed. (top) Digital image of a portion of the tidal flats in the northern lagoon of Venice, localized within the lagoon (the *forma urbis* of the city of Venice appears in the bottom part of the uppermost left inset). Also shown is the automatic extraction of the channelized patterns, to scale, according to the techniques described by *Fagherazzi et al.* [1999a]. (bottom) Planar geometry of seven meandering tidal channels (out of approximately 150 within our database), extracted, respectively, from the lagoon of Venice (Italy) (VE1, VE2, VE3); Barnstable (MA, USA) (BA1, BA2); and Petaluma (CA, USA) (PE1, PE2). It is seen the wide range of scales and of degrees of meandering sampled. Notice that the patterns are represented to scale, and that the pixel size varies from case to case, as described by *Fagherazzi et al.* [1999a] and *Rinaldo et al.* [1999a, 1999b].

ders from observed data, even though, in some circumstances, it might introduce spurious wavelengths due to inaccuracies in the computation of the curvature. Such ambiguities must be resolved by a suitable operator, defined in the following. The planar characterization of a meandering channel is completed by its half width $B(s)$ (Figure 2) which contains crucial information also on the magnitude of landscape-forming flow rates shaping its cross-sections.

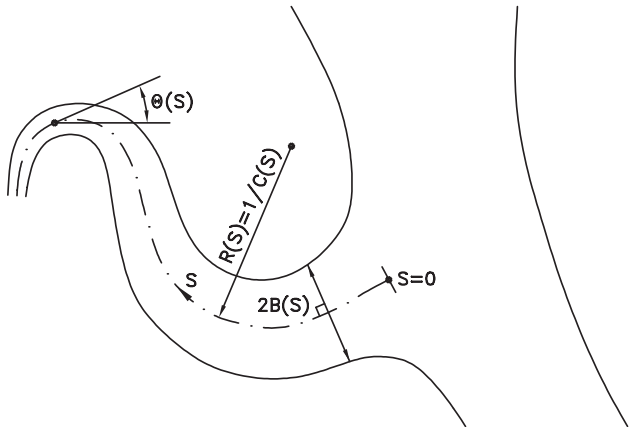

Figure 2. Sketch of a tidal meander showing the parameters describing the geometry of a meandering channel.

Indeed we shall see that the planar development of widths carries significant geomorphological information.

[11] Focusing our attention on the geometry of the channel axis, the established framework of reference in fluvial geomorphology [e.g., *Kinoshita*, 1961; *Leopold et al.*, 1964; *Ikeda et al.*, 1981; *Seminara et al.*, 2001] expresses, on theoretical and observational grounds, the shape of fluvial meanders in the idealized form:

$$c(s) = c_0\left[\cos\frac{2\pi s}{L_s} - c_F\cos\,3\frac{2\pi s}{L_s} - c_S\sin\,3\frac{2\pi s}{L_s}\right] \qquad (1)$$

where c_F and c_S are, respectively, the fattening and skewness coefficients. It is noticed that the second harmonic is absent in (1), which refers to an ideal case, in which the third harmonic components are responsible for the fattening (c_F) and skewing (c_S) of meander lobes. It should be noticed that, in the fluvial case, the lack of even harmonics (i.e., the second ones) is the result of the cubic geometric nonlinearity of the planimetric evolution equation [e.g., *Seminara et al.*, 2001].

[12] In order to place the study of tidal meanders in a proper theoretical framework, such as through equation (1), it is necessary to analyse the spectral properties of the observed channel axes. This, in turn, must be based on a discretized representation $x_k = x(s_k)$, $y_k = y(s_k)$ ($s_k = k\Delta s$) of the axis $x(s)$, $y(s)$ obtained from the data of Figure 1 through a ''skeletonization'' procedure [e.g., *Fagherazzi et al.*, 1999a; *Zandolin*, 1999]. The analyses presented in this paper are based on the numerical determination, from observations, of the functions $\theta(s)$ (angle formed by the tangent to the axis and the horizontal direction, Figure 2) and $c(s)$ through the elementary relationship:

$$c(s) = -\frac{d\theta(s)}{ds} = \frac{(dx/ds)(d^2y/ds^2) - (dy/ds)(d^2x/ds^2)}{\left[(dx/ds)^2+(dy/ds)^2\right]^{3/2}} \qquad (2)$$

which reduces the problem to the numerical computation of the derivatives in equation (2). Once the discretized function $c_k = c(s_k)$ is determined, its discrete Fourier tranform (DFT) may be easily performed. The approach requires accurate approximation techniques as discretization errors are amplified in the computation of derivatives of progressively increasing order. Suffice here to note that the discrete set of observational points implies the use of discrete Fourier transforms (DFT), which allow fast and accurate manipulations, explicit control of aliasing and of the spatial scales filtered.

[13] An interpolation ($\hat{x}(s)$, $\hat{y}(s)$) of the series of N meander sites x_k, y_k is first obtained through the discrete Fourier transforms X_n, Y_n:

$$\hat{x}(s) = \frac{1}{N}\sum_{n=0}^{N-1} X_n\, e^{i2\pi ns/N} \qquad (3)$$

and likewise for $\hat{y}(s)$, Y_n. By deriving, say the component $\hat{x}(s)$ one obtains:

$$\frac{d\hat{x}(s)}{ds} = \frac{1}{N}\sum_{n=0}^{N-1}\frac{i2\pi n}{N} X_n\, e^{i2\pi ns/N}$$

$$\frac{d^2\hat{x}(s)}{ds^2} = \frac{1}{N}\sum_{n=0}^{N-1} -\left(\frac{2\pi n}{N}\right)^2 X_n\, e^{i2\pi ns/N} \qquad (4)$$

[14] Analogous expressions are found for $\hat{y}(s)$. Equations (4) allow the estimation of first and second order derivatives of $\hat{x}(s)$ and $\hat{y}(s)$ and the filtering of the signals at a specified wavelength. Equations (4) and (2) may be used to compute the values $c(s_k)$ on the discrete set of points $s_k = k\Delta s$, and consequently to determine the position of inflection points.

[15] A final theoretical development is required to describe how skewed a tidal meander may become as a result of a progression of the lateral migration of its inner and outer banks (whether or not similarly to the accepted fluvial mechanism that conserves widths owing to a balance of erosion and deposition along the radius of curvature [e.g., *Ikeda et al.*, 1981; *Blondeaux and Seminara*, 1985]). Since we carry out the spectral analysis without neglecting even modes like in the Kinoshita model, equation (1), the meaning of flatness and skewness must be clarified in the general case. It will be shown later that modes higher than the third play a decidedly minor role in shaping observed tidal meanders. Therefore in the following we analyse an expression of the curvature that includes even modes and introduce a more general analytical scheme than that described by equation (1), i.e.:

$$c(s) = R_1\cos(s) + I_1\sin(s) + \varepsilon[R_2\cos(2s) + I_2\sin(2s) + R_3\cos(3s) + I_3\sin(3s)] \qquad (5)$$

where a function containing only a single harmonic is perturbed by a second and a third component, ε is a 'small' parameter and R_2, I_2, R_3 and I_3 are of the same order as R_1 and I_1 (to ensure that the perturbation is 'small'). Notice that the actual value of total meander length (2π in this case) is immaterial as the intrinsic component may be rescaled without loss of generality. Let us first consider the zero order problem in which $\varepsilon = 0$. We are interested in finding the inflection points with intrinsic coordinates σ_{0k} delimiting each meander (Figure 3) and defined by the condition $c(\sigma_{0k}) = 0$. We are also interested in determining the coordinates τ_{0k} of the apexes, i.e., the points where the curvature has a local extreme, defined by $dc/ds|\tau_{0k} = 0$. Their position relative to the neighboring inflection points

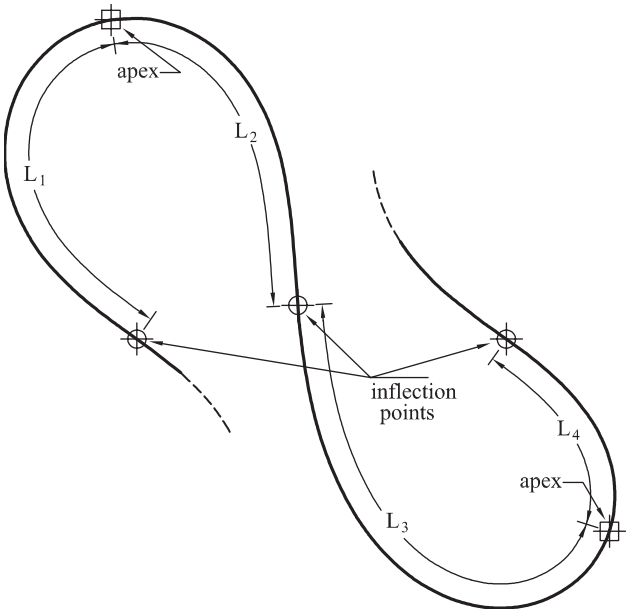

Figure 3. Geometrical characterization of a meander through inflection points and lobe lengths. In general, skewness is defined by the asymmetry in the lengths between subsequent apexes and inflections points as shown herein ($L_1 > L_2$, $L_3 > L_4$).

contain information as to the symmetry/asymmetry of a meander (Figure 3). Solution of the equations for σ_{0k} and τ_{0k} in the zero-order problem ($\varepsilon = 0$) yields:

$$\sigma_{0k} = tan^{-1}\left(-\frac{R_1}{I_1}\right) + k\pi; \quad k = 0, 1, \ldots$$
$$\tau_{0k} = tan^{-1}\left(\frac{I_1}{R_1}\right) + k\pi; \quad k = 0, 1, \ldots \tag{6}$$

[16] For the properties of the tangent it is:

$$\tau_{0k} = \sigma_{0k} + \frac{\pi}{2} \tag{7}$$

[17] In the case of $\varepsilon = 0$ the meander defined by (5) is thus symmetric as each lobe, of length π, is divided by the apexes into two parts of equal length $\tau_{0k} - \sigma_{0k} = \pi/2$.

[18] We now seek to understand how the positions of the inflection points and of the apexes are changed by the introduction of the second and third harmonic components in expression (5). Their intrinsic coordinates may be expressed as $\sigma_k = \sigma_{0k} + \varepsilon\sigma_{1k}$ and $\tau_k = \tau_{0k} + \varepsilon\tau_{1k}$ since their displacement with respect to σ_{0k} and τ_{0k} should be of the same order as the perturbation in equation (5). Such coordinates may be determined by finding the zeros of the equations:

$$c(\sigma_k) = c(\sigma_{0k} + \varepsilon\sigma_{1k} + \ldots) = 0$$
$$\left.\frac{dc}{ds}\right|_{\tau_k} = \left.\frac{dc}{ds}\right|_{\tau_{0k}+\varepsilon\tau_{1k}+\ldots} = 0 \tag{8}$$

[19] The expansion of equations (8) around σ_{0k} and τ_{0k}, once the terms of order higher than the first are discarded, yields:

$$\begin{aligned}
&\sigma_{1k}[-R_1\sin(\sigma_{0k}) + I_1\cos(\sigma_{0k})] + R_2\cos(2\sigma_{0k}) + I_2\sin(2\sigma_{0k}) \\
&\quad + R_3\cos(3\sigma_{0k}) + I_3\sin(3\sigma_{0k}) = 0 \\
&\tau_{1k}[-R_1\cos(\tau_{0k}) - I_1\sin(\tau_{0k})] - 2R_2\sin(2\tau_{0k}) + 2I_2\cos(2\tau_{0k}) \\
&\quad - 3R_3\sin(3\tau_{0k}) + 3I_3\cos(3\tau_{0k}) = 0
\end{aligned} \tag{9}$$

[20] The solutions to these equations may be expressed (using relation (7)) as follows:

$$\sigma_{1k} = \frac{R_2\cos(2\sigma_{0k}) + I_2\sin(2\sigma_{0k}) + R_3\cos(3\sigma_{0k}) + I_3\sin(3\sigma_{0k})}{R_1\sin(\sigma_{0k}) - I_1\cos(\sigma_{0k})} \tag{10}$$

$$\tau_{1k} = \frac{-2R_2\sin(2\sigma_{0k}) + 2I_2\cos(2\sigma_{0k}) - 3R_3\cos(3\sigma_{0k}) - 3I_3\sin(3\sigma_{0k})}{R_1\sin(\sigma_{0k}) - I_1\cos(\sigma_{0k})}$$

[21] The presence of the second and third harmonics displaces the position of the apexes with respect to the inflection points, thus changing the lengths L_1, L_2 of the two portions in which the lobes are divided (Figure 3). Such lengths may now be used to quantitatively express upstream and downstream skewing of the meanders. In particular, with reference to Figure 3, the first lobe of the meander will be said to be downstream skewed when $L_1 > L_2$ and upstream skewed when $L_1 < L_2$. We thus introduce the following ratio to quantify meander skewing:

$$\frac{L_1}{L_2} = \frac{\tau_0 - \sigma_0}{\sigma_1 - \tau_0} = \frac{\frac{\pi}{2} + \varepsilon L_{11}}{\frac{\pi}{2} + \varepsilon L_{21}} \tag{11}$$

[22] Where:

$$L_{11} = \frac{(2R_2 + I_2)\sin(2\sigma_{00}) + (R_2 - 2I_2)\cos(2\sigma_{00}) + 4R_3\cos(3\sigma_{00}) + 4I_3\sin(3\sigma_{00})}{-R_1\sin(\sigma_{00}) + I_1\cos(\sigma_{00})}$$

$$L_{21} = \frac{(-2R_2 + I_2)\sin(2\sigma_{00}) + (R_2 + 2I_2)\cos(2\sigma_{00}) - 4R_3\cos(3\sigma_{00}) - 4I_3\sin(3\sigma_{00})}{-R_1\sin(\sigma_{00}) + I_1\cos(\sigma_{00})}$$

[23] Equation (11) allows the definition of the shape parameter:

$$\chi = \frac{L_{11}}{L_{21}} = \frac{(2R_2 + I_2)\sin(2\sigma_{00}) + (R_2 - 2I_2)\cos(2\sigma_{00}) + 4R_3\cos(3\sigma_{00}) + 4I_3\sin(3\sigma_{00})}{(-2R_2 + I_2)\sin(2\sigma_{00}) + (R_2 + 2I_2)\cos(2\sigma_{00}) - 4R_3\cos(3\sigma_{00}) - 4I_3\sin(3\sigma_{00})} \tag{12}$$

[24] A value $\chi > 1$ indicates downstream skewing of the meander, while $\chi < 1$ characterises upstream skewing. Expression (12) constitutes a way of characterizing upstream/downstream skewing of observed meanders as R_2, I_2, R_3 and I_3 may be estimated by Fourier transforming the function $c(s)$ computed through equations (4) and (2).

[25] It should be noticed that the deformation of the lobes with respect to the zero-order case is such that the lengths of the lobes $L_1 + L_2 = \sigma_1 - \sigma_0 = L_3 + L_4 = \sigma_2 - \sigma_1 = \pi$ are kept constant as well as the total length $L_T = \sigma_2 - \sigma_0 = 2\pi$.

[26] We now note that expression (5) may be manipulated by use of elementary trigonometric results to eliminate the imaginary part, I_1, of the first mode by introducing a suitable phase angle which only changes the origin of the intrinsic coordinate s. It is in fact well known that a rotation of the Fourier transform of a function corresponds to a rigid shift of the function in physical space. We may therefore

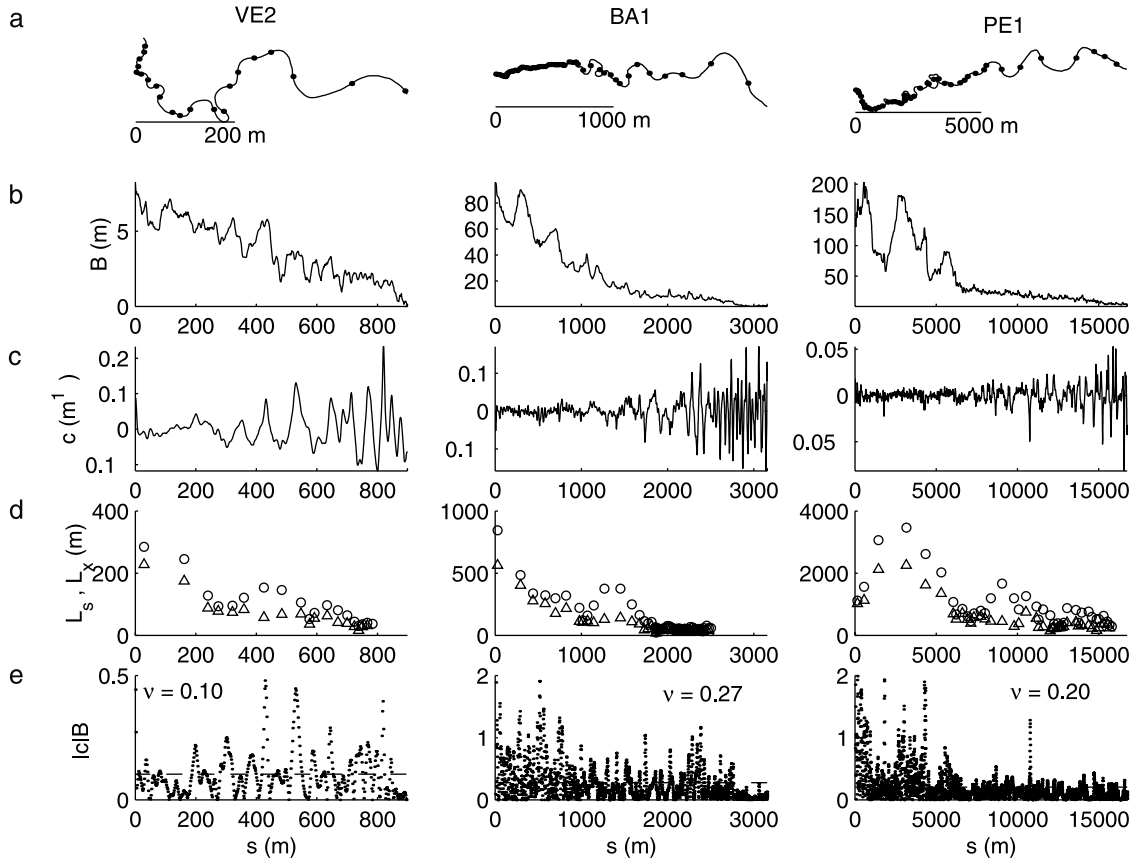

Figure 4. (a) Channel axis configuration, (b) half width, (c) curvature, (d) intrinsic and Cartesian meander lengths, and (e) product of the absolute value of the curvature by half width for three of the channels considered. They are channels VE2, BA1, and PE1 of Figure 1, namely, within the Venice Lagoon, the Barnstable salt marsh, and Petaluma bay.

assume, without loss of generality, that the curvature be expressed as:

$$c(s') = R_1' \cos(s') + \varepsilon\left[R_2' \cos(2s') + R_2' \sin(2s') + R_3' \cos(3s') + I_3' \sin(3s')\right] \tag{13}$$

which is similar to (1). Notice that, from (6), $\sigma_{00} = -\pi/2$ and thus the shape parameter χ now takes the form:

$$\chi = \frac{R_2' - (2I_2' + 4I_3')}{R_2' + (2I_2' + 4I_3')} \tag{14}$$

[27] Expression (14) shows that the real part, R_2', of the second mode does not induce any skewing of the meander as only if $I_2' \neq 0$ or $I_3' \neq 0$ may be $\chi \neq 1$. It is also seen that the real part of the third mode, R_3', does not affect skewing in any manner, at least in the first-order approximation adopted here.

3. Results

[28] Figure 4 shows a synthesis of our observations for channels from the lagoon of Venice (Pagliaga salt marsh), Barnstable marsh and Petaluma Bay. Here we choose to show (1) the planar trace of the centerline of the meanders, with indications on the sites of the inflection points; (2) the spatial evolution (i.e., alongstream) of the half widths $B(s)$. The latter quantity is computed by determining the curves delimiting the channelized areas (to the left and to the right of the axis) and by determining the distance between the intersections of such curves with the line orthogonal to the axis at every (discretized) centerline site s_k (see Figure 2) (for computational details, see *Fagherazzi et al.* [1999a]). The range of the measured values of $B(s)$ varies considerably and one notes that estimates tend to be affected by significant error only in the narrower channels, where the width becomes comparable with the pixel size; (3) the spatial evolution of the curvature $c(s)$, computed by the spectral approach described earlier; (4) the spatial development of intrinsic, L_s, and Eulerian, L_x, meander wavelengths; and (5) the evolution of the dimensionless product of half width and curvature (in absolute value). From Figure 4 several observations can be drawn.

[29] Both meander widths and wavelengths increase substantially seaward (Figures 4b and 4d), exhibiting fluctuations which are at times noteworthy. Thus the observational signals constructed by using the intrinsic coordinate s are nonstationary. In particular, the trend shown by the curvature in Figure 4c is characterized by high frequency fluctuations which are part of the signal in the narrower reaches of the channels (i.e., landward) and are part of the noise near the mouth (i.e., as s approaches zero). From an operational

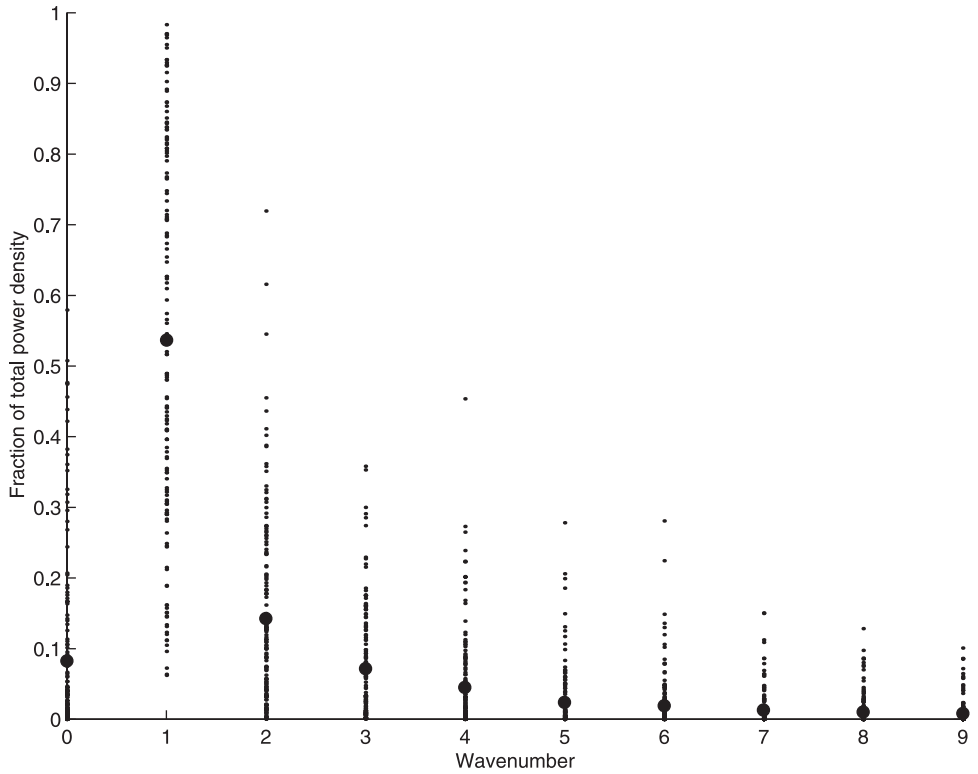

Figure 5. Power spectrum for all the channels analyzed. Solid circles denote average values for each wave number.

point of view, this setup implies that a low-pass filter threshold, which effectively eliminates noise in the landward portions of the channels, is unable to filter out noise near the mouth. This circumstance can be properly accounted for by increasing the filtering wavelength as the width increases. Indeed, from a geometrical point of view, the values which can be attained by the curvature of the axis are somewhat related to channel width. For rather small widths sharp 'turns' are in principle allowed. On the contrary, when the width increases, only smaller curvatures are possible in order to avoid the creation of oxbows. The spatial development of the dimensionless product $\nu = |c(s)|$ $B(s)$ shown in Figure 4e exhibits fluctuating patterns which, however, maintain a nearly constant mean value ($\bar{\nu} \sim 0.2 \pm 0.1$). This seems to substantiate the existence of the relationship between curvature and width discussed above. Furthermore, the relatively small value attained by $\bar{\nu}$ indicates that tidal channels are not too strongly meandering. Such circumstance allows an analytical treatment of the morphodynamic problem in tidal channels as in *Solari et al.* [2002], where a linear solution is obtained for the flow field and the bed topography and the planimetric instability theory developed by *Blondeaux and Seminara* [1985] for river meanders is extended to tidal environments.

[30] As described in Section 2, the proposed approach allows the automatic delimitation of meanders within the analyzed channels by finding the zeroes of $c(s)$, i.e., the inflection points of the meander centerline. A channel reach containing three such inflection points is defined as a meander. The analysis may now proceed by testing the ideal fluvial model equation (1) against tidal channel data by Fourier analyzing (i.e., by discrete Fourier transformation) the curvature $c(s)$, periodic of period L_s, for each meander. Figure 5 shows the power spectra, normalized to the total power density, of all the meanders considered. The binned average values of the dimensionless power density corresponding to each wave number, indicate that the energy associated to the first three/four harmonics is dominant. The decay of spectral energy toward higher modes proves indeed smooth suggesting convolutive (nonlinear) interactions among modes. Moreover, unlike in *Kinoshita*'s [1961] curve (equation 1), the power density of the second harmonic is not negligible, its average value being greater than the value associated with the third harmonic. The dependence of the first three harmonics of the power spectrum on the intrinsic coordinate s for all the channels analyzed (not shown here for brevity) shows that, despite the presence of fluctuations, the power density maintains a nearly constant value along any given channel. This relates to the fact that, as the intrinsic wavelength increases seaward, the corresponding curvature values proportionally decrease. The ratio of the energy of the second to the first harmonic (as well as the ratio of the energy of the third harmonic to the first) seems independent of the intrinsic coordinate s, thus suggesting a local adaptation of meander morphology to changes in hydrodynamic conditions reflected by the increasing widths and wavelengths.

[31] The presence of the second harmonic in the energy spectra of tidal meanders poses a fundamental interpretational problem. Fluvial meanders, in fact, typically exhibit a certain degree of fattening and are usually upstream skewed, a feature which allows one to detect flow direction from aerial photos. Nevertheless, some observational evidence exists indicating that in some circumstances meander lobes

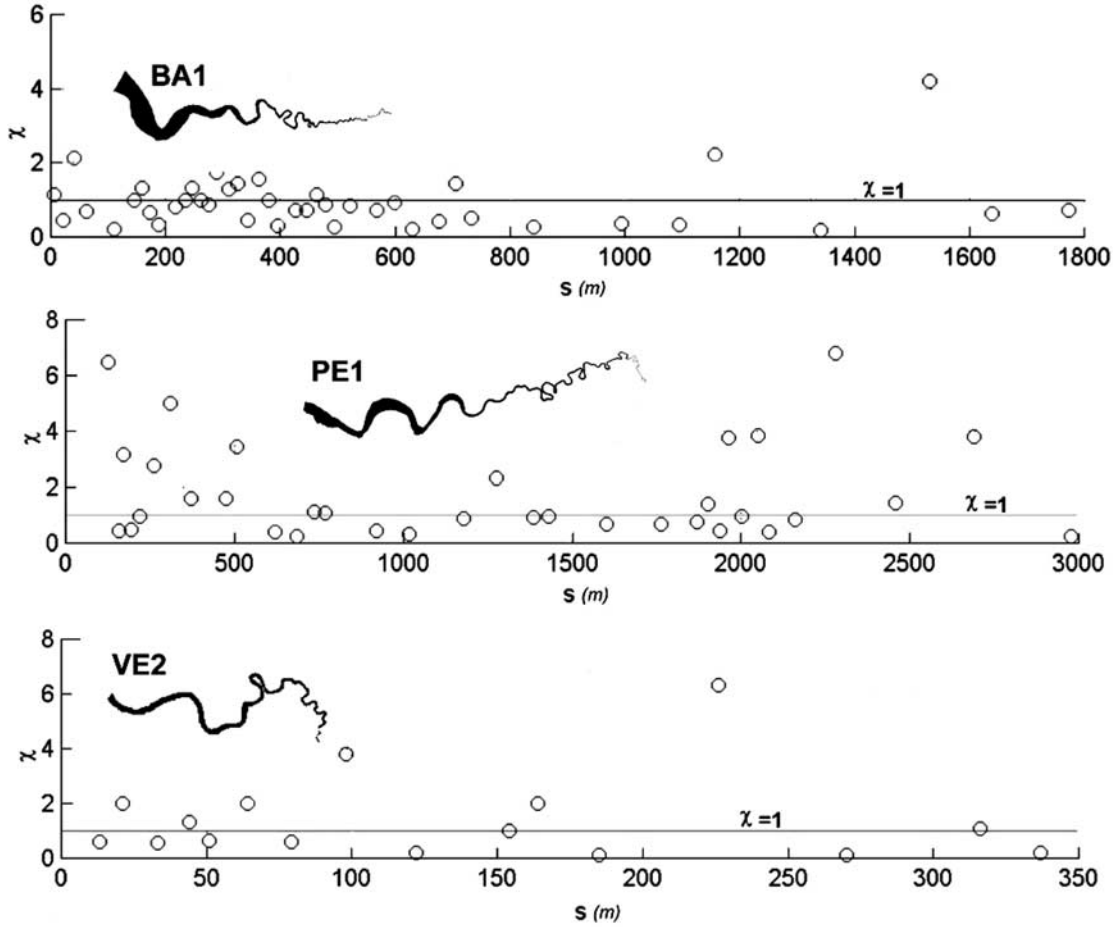

Figure 6. The morphological parameter χ (defined by equation (14)) as a function of the intrinsic coordinate for the three environments described in Figure 4.

can be also downstream skewed. Kinoshita's curve seems to satisfactorily capture these basic features. For unconfined meanders, the absence of even harmonics (included the second one), and the negligibility of harmonics higher than the third embodied by Kinoshita's curve has a theoretical justification. The mechanistic model of the planimetric evolution of river meanders formulated by *Seminara et al.* [2001], in fact, indicates that the absence of even harmonics is strictly related to the cubic nonlinearity in the integro-differential equation which governs the planimetric evolution, where the radial velocity of displacement of the axis is linked, to first-order, to the local curvature. In particular, Langbein and Leopold's sine generated curve and Kinoshita's curve turn out to be the leading, and the second order, approximation of the exact solution of the above planimetric evolution equation, respectively. The third harmonic thus arises as a result of nonlinear interactions and its role increases as the meander fully develops. *Seminara et al.* [2001] have also shown that, in accordance with empirical observations, fluvial meanders may indeed result upstream or downstream skewed depending on the value attained by the width to depth ratio β. When β is smaller than the resonant value β_R of *Blondeaux and Seminara* [1985] (i.e., the value of β for which the growth rate of a sequence of regular meanders tends to infinity) meanders result upstream skewed and migrate downstream. On the contrary,

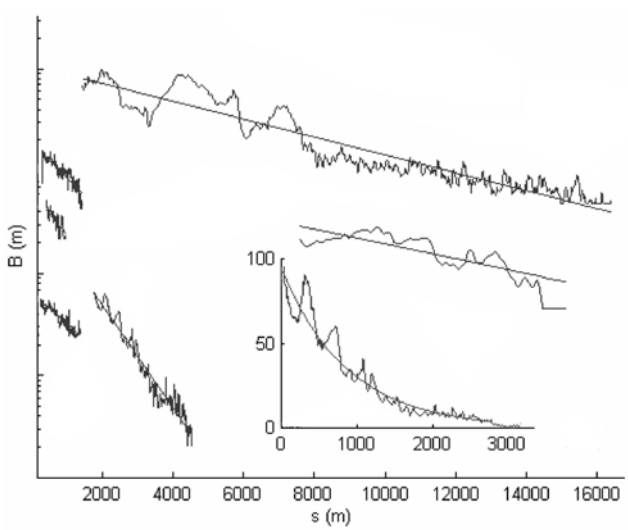

Figure 7. Logarithm of the half width of the channels analyzed versus the intrinsic coordinate *s*. It is seen through the fit of a straight line in the semilog plot how *B* increases approximately exponentially.

Table 1. Values of the e-folding Length of Channel Width L_B for Various Channels Located in the Northern Part of the Venice Lagoon (A), in Pagliaga Salt Marsh (B), in Barnstable (C, D, and E), and in Petaluma (F and G)

	Channel						
	A	B	C	D	E	F	G
L_B (m)	5300	1400	2900	4850	4700	10700	8000
L_c (m)	16775	1070	6769	2671	1157	18100	3970

when β is higher than its resonant value, downstream skewing develops. Such configurations correspond, in the representation yielded by equation (1), to positive or negative values of the coefficient c_S, respectively.

[32] The analysis of the spectra computed from all the environments considered shows the inadequacy of the above picture for tidal meanders, the amplitude associated with the second harmonic being significant. As a consequence, we resort to the definitions in equation (12) of more involved skewness and fattening factors to interpret the observational patterns. In principle this morphological parameter allows one to detect the possible existence of a preferential skewness direction of tidal meanders indicating whether bank erosion phenomena governing meander migration are controlled by either flood or ebb flow. Indeed, meander point bars have been observed to be asymmetrically disposed on the meander bend if there is one dominant flow direction [*Barwis*, 1978; see also *Dalrymple and Rhodes*, 1995]. Thus the study of the skewness offers, through the computation of the parameter χ, a chance of detecting on a purely morphological basis the existence of a transition in the hydrodynamic regime from flood-dominated areas (where the duration of falling tides exceeds that of rising tide, producing longer lags at low water than high water, and leading to a tendency for stronger flood than ebb tidal currents) to ebb-dominated regions (where the opposite situation occurs; see *Friedrichs and Aubrey* [1988] for a thorough discussion of flood and ebb dominance).

[33] The parameter defined by (12) may be estimated for actual channels by the above Fourier analysis. Figure 6 shows sample results of such a computation for the channels in Figure 4. It is seen how the values computed do not show any obvious pattern as a function of the intrinsic coordinates. Thus the possibility of detecting a morphological signature of changing hydrodynamic regimes proves elusive, at least on the basis of our data. This result might be justified observing that, unlike in fluvial meanders, the asymmetry possibly induced by the dominant flow is likely

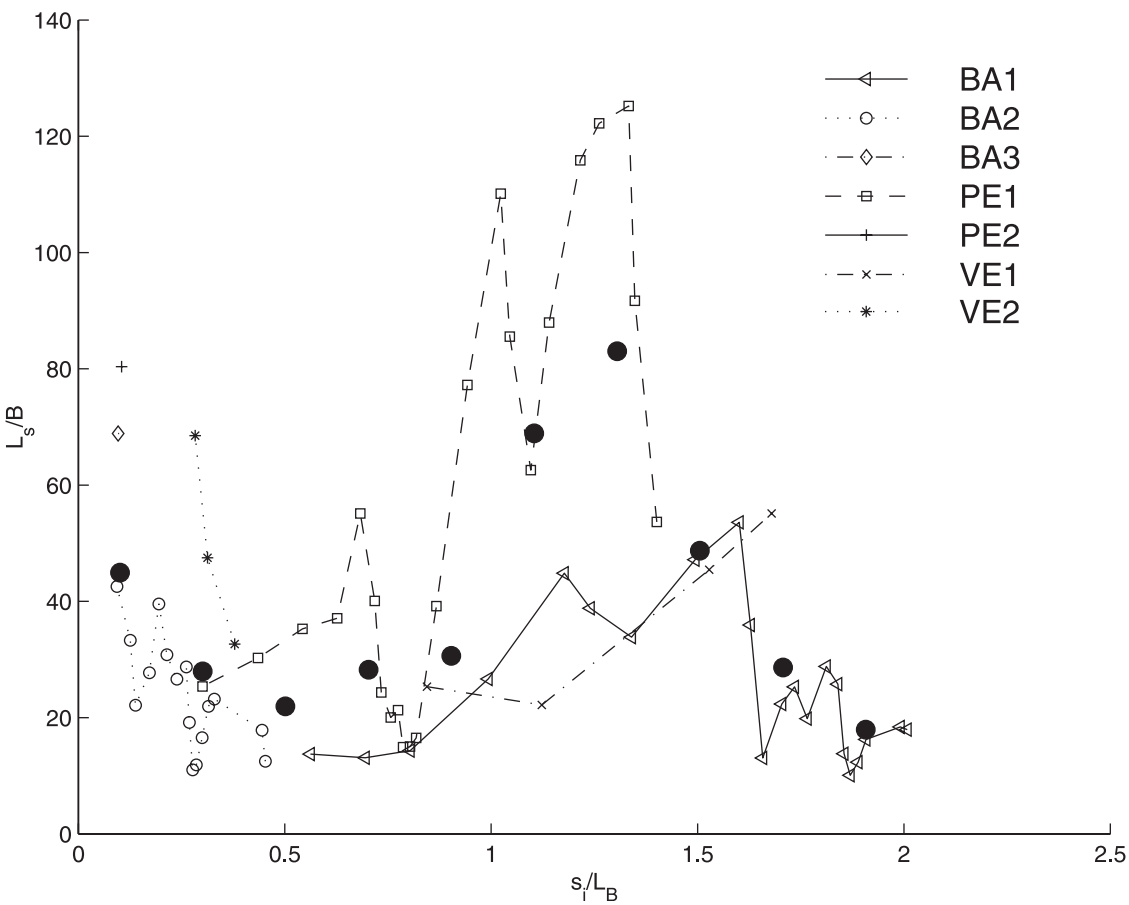

Figure 8. Spatial development of dimensionless wavelengths. The ratio $L_s/\bar{B}$ is plotted versus s_i/L_B for all the channels analyzed. Data are considered only when the width exceeded twice the size of the pixel of the topographic description. The legend indicates the environment from which the data were taken (BA, Barnstable; BA1, BA2, BA3, different meanders within the Barnstable saltmarsh; PE, Petaluma; VE, Venice). Solid dots represent binned average values.

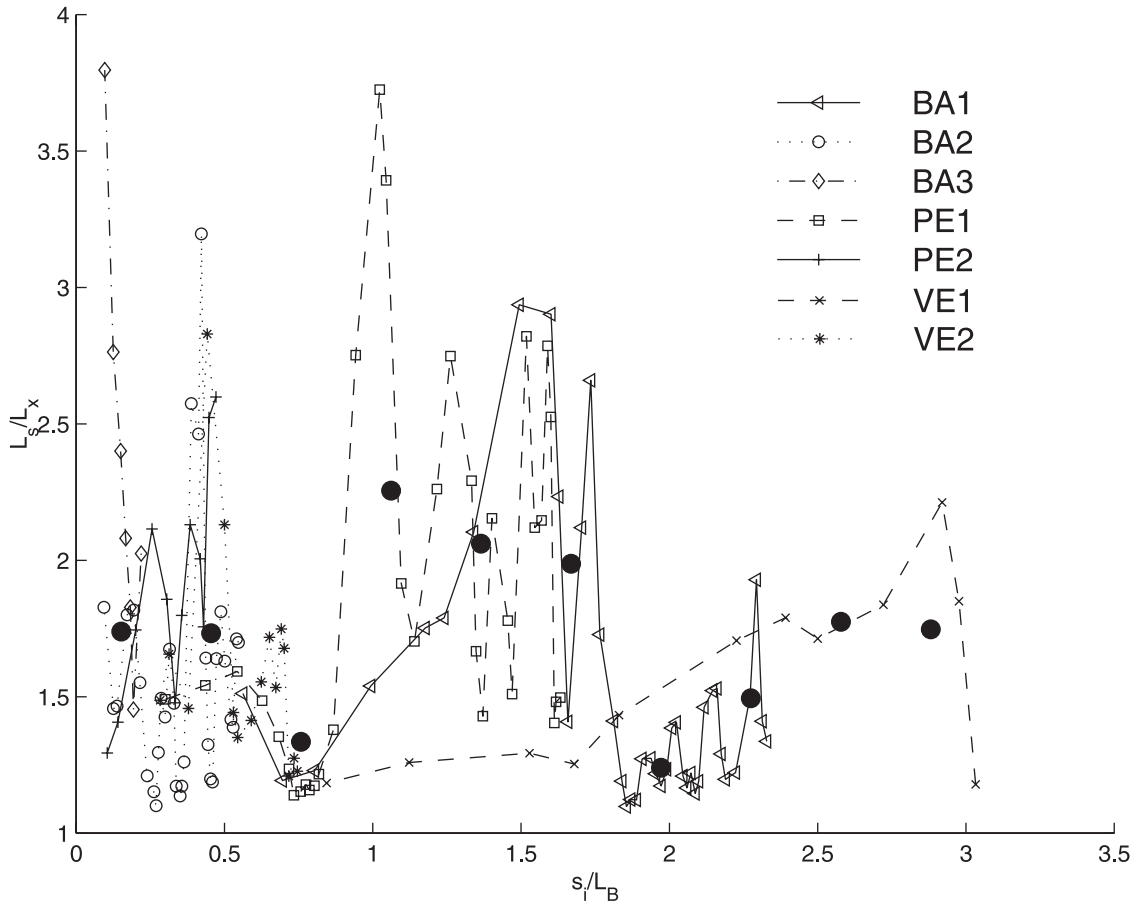

Figure 9. Spatial development of sinuosity, L_s/L_x, plotted versus s_i/L_B, for the channels analyzed in Figure 8. The legend is as in Figure 8. Solid circles denote binned average values.

to be rather weak owing to the oscillating character of the flow field. Furthermore, it must be ascertained whether the tidal environments investigated actually exhibits a transition between the two different tidal regimes defined above. We do not have sufficient information on the hydrodynamic features in the environments considered to make such a distinction.

[34] The spatial variability of channel characteristics is further explored in Figure 7, showing the semi-log plot of half width $B(s)$ versus the intrinsic coordinate s for the channels of Figure 1. It is noteworthy that the seaward growth of $B(s)$ is very nearly exponential, i.e., $B \sim B_0 \exp(-s/L_B)$, where B_0 is the initial width at $s = 0$. The values of L_B obtained for the channels in Figure 1 (i.e., the inverse of the slope of the plots) and their lengths L_c are reported in Table 1. The values of the ratio L_B/L_c fall in a range comparable with that typically observed in fluvial estuaries [e.g., *Lanzoni and Seminara*, 1998]. It is interesting to note that, even though L_B changes from channel to channel with no apparent regularity, a tendency seems to emerge for which shorter creeks tend to be characterized by larger values of the above ratio. This observation bears implications on the aggregation patterns leading to the formation of the dominant flow discharges.

[35] Dimensional analysis may be used to identify the dimensionless parameters needed to describe the planar geometry of tidal meanders and to free the description from the dependence on the absolute magnitude of the dimensional parameters introduced. Five dimensional parameters may be introduced to characterise the planar geometry of a tidal meander: L_x, L_s, $\bar{B}$, B_0, L_B, s_i, where $\bar{B}$ is the average channel width within a meander and s_i is its initial coordinate introduced to to characterise the variability in space of meander properties. The quantities listed depend on only two fundamental scales. A scale along the intrinsic coordinate direction, which characterises the variability over scales larger than single meanders, and a scale in the direction orthogonal to the axis, typical of the processes occurring within each meander. According to the fundamental theorem of dimensional analysis (e.g., *Langhaar*, 1951) the problem may thus be described in terms of four dimensionless parameters. An appropriate choice of such parameters may be: $L_x/\bar{B}$, $L_s/\bar{B}$, $\bar{B}/B_0$, s_i/L_B. The results of Figure 7 indicates that $\bar{B}/B_0$ and s_i/L_B are not independent. In fact, by computing the average width of a generic meander one finds:

$$\bar{B} = B_0 \frac{L_B}{L_s}[1 - \exp(-L_s/L_B)]\exp(-s_i/L_B) \qquad (15)$$

[36] The value of L_B is found to be much larger than meander lengths (in our data $L_s/L_B \sim 0.1$). This is not surprising as the increase in channel width, which *Rinaldo et al.* [1999a, 1999b] link to the increase in the discharge

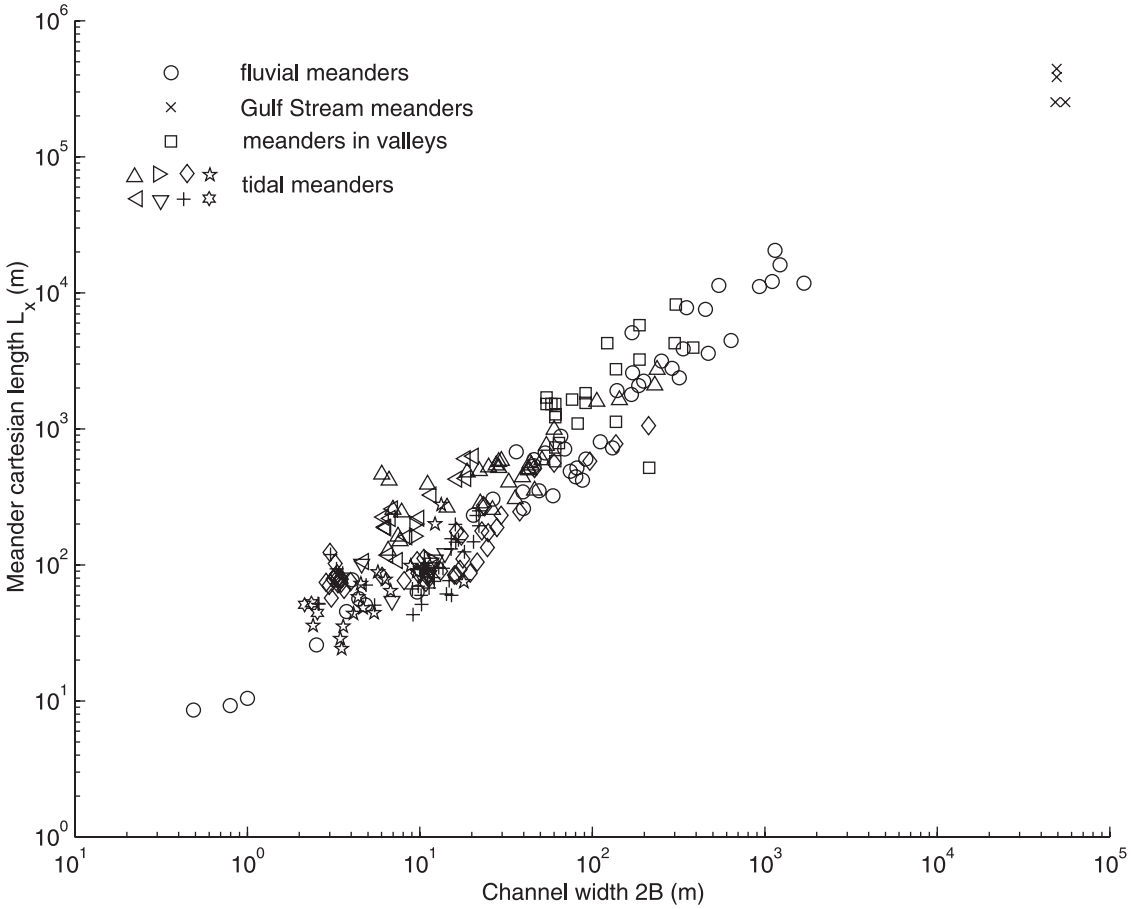

Figure 10. Cartesian meander length versus width for rivers (circles), fluvial valleys (squares), and the gulf stream (crosses) [after *Leopold et al.*, 1964] compared to tidal meanders from this database (portrayed by the different symbols shown in the inset). Notice the different symbols pertaining to the development of the same tidal meander, corresponding to sites along the same observed pattern where width and amplitude have been measured. It is remarkable that a roughly constant ratio is maintained. The fact that the fluctuations induced by tidal patterns are no larger than those observed for such diverse morphologies as valleys, glaciers, and the gulf stream is deemed suggestive.

shaping channel cross sections, occurs over scales larger than those characteristic of wall erosion processes shaping meander geometry. As consequence, since L_s/L_B approaches zero in (15), $\bar{B}/B_0$ has an exponential, one-to-one, dependence on s_i/L_b. This finding further reduces the number of dimensionless parameters to three, as one may express the spatial variability of the parameters $L_x/\bar{B}$ and $L_s/\bar{B}$ by studying their behaviour with respect to s_i/L_B.

[37] The changes of the intrinsic dimensionless wavelength, $L_s/\bar{B}$, and of sinuosity, L_s/L_x, as a function of s_i/L_B are plotted in Figures 8 and 9 for all the channels analyzed. It is seen how almost all the binned values of the ratio $L_s/\bar{B}$ remains confined in the range 20-40 despite the length scales L_s and $\bar{B}$ grow significantly (e.g., by more than two orders of magnitude in the case of Petaluma). Figure 9 shows that the binned values of the sinuosity fall within the quite narrow interval $1.3 < L_s/L_x < 2.2$, i.e., a range of values smaller than that typically observed in fluvial meanders. The limited range exhibited seems to suggest that a similarity of shapes exists between meanders of different sizes and that a single property (e.g., the intrinsic wavelength) suffices in describing the 'longitudinal' geometric characteristics of the tidal meanders analyzed herein.

[38] An interesting relationship between two of the parameters introduced above may be obtained by considering an empirical result known for fluvial environments, which relates the cartesian meander length to the channel width [e.g., *Leopold et al.*, 1964]. Figure 10 shows observations [after *Leopold et al.*, 1964, Figures 7.41a and 7.46] from (1) different fluvial environments; (2) valleys left by ancient river courses, or relics of past wetter climates; and (3) gulf stream meanders, to which our data on tidal meanders have been added. The data indicate the validity of a linear relationship $L_x \propto B$, as observed by *Leopold et al.* [1964]. It is relevant that the new data from our observations do not modify appreciably, within statistical significance, the linear relationship between L_x and $\bar{B}$. The dimensionless parameter $L_x/\bar{B}$ thus tends to be constant across very different environments. This suggests that when the physical mechanisms governing the spatial development of meanders act at a scale comparable with their width, the landforms generated exhibit strong similarities independently of the nature of the processes that shape them.

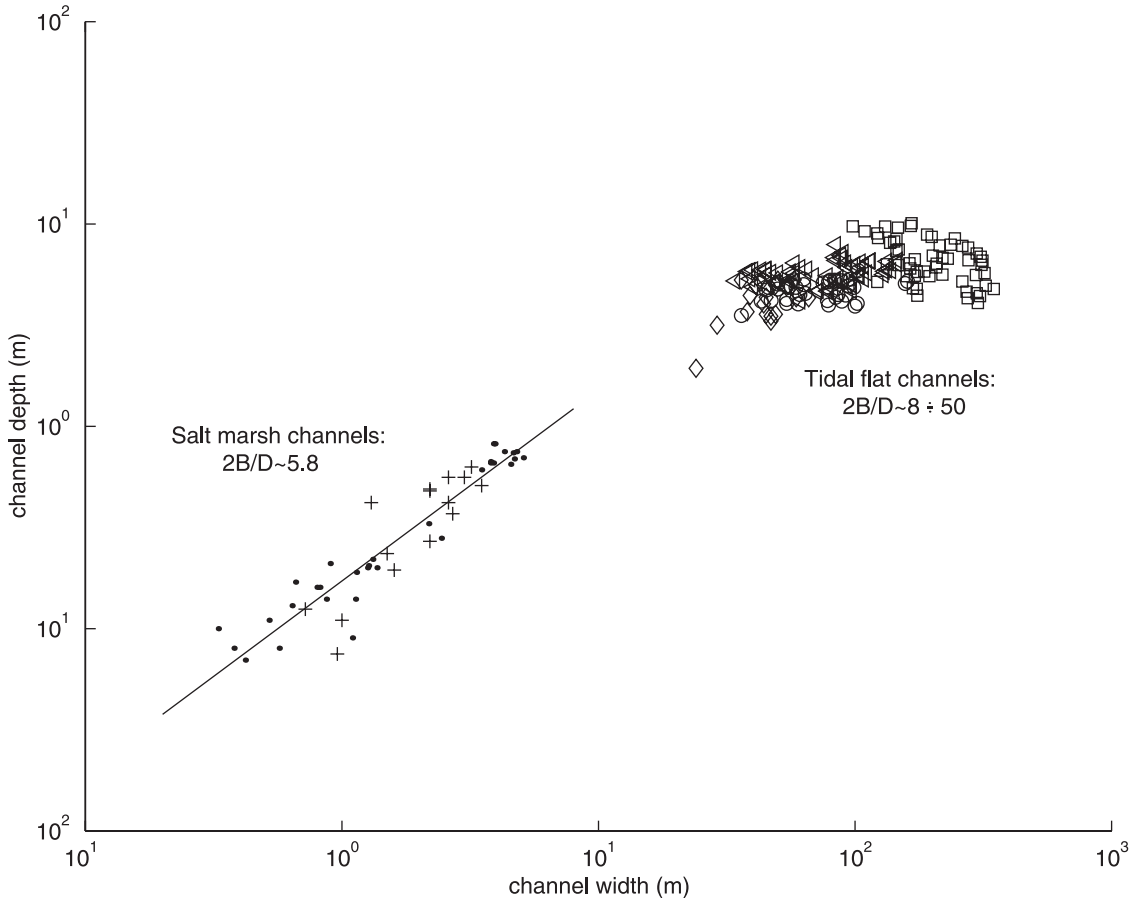

Figure 11. Width versus depth for a number of directly surveyed tidal channel sections in the lagoon of Venice. Crosses and dots indicate two different salt marsh channels measured along their winding path. Diamonds, squares, and triangles indicate tidal flat channels. As an excercise, we have fitted only salt marsh data with a straight line (whose intercept is forced to zero), which is estimated to yield a slope $\beta \sim 6$ and $R^2 = 0.98$.

[39] A comparative study of fluvial and tidal forms can be based on the above features. Specifically, we applied the techniques of analysis introduced here to mesoscale landforms observed within the river Livenza in northern Italy. We analyzed three different reaches of lengths 4700, 6700 and 19900 m respectively, characterized by mean discharge values of 16, 50 and 90 $m^3 s^{-1}$, and mean widths of 20, 25 and 50 m. Negligible spatial gradients of contributing area suggest constant landforming flow rates within each of the reaches considered. We found that, differently from the tidal cases, meander wavelengths are approximately constant as well as the ratio of wavelength to width. Further, computation of the parameter χ in equation (14) indicates consistent up-stream skewing of the meanders ($\chi < 1$). The comparison of the fluvial and tidal forms therefore indicates that in the latter cross-sectional dimensions are strongly varying in space in response to strong discharge gradients. It is remarkable, however, that the proportionality of wavelength and width applies in both cases. On this basis alone we might suggest that a condition of local equilibrium should hold even in tidal environments, in which the average width of each meander and its cartesian length adjust to the value of the dominant discharge with no appreciable (and durable) transient feature moving from one meander lobe to the next ones.

[40] Finally, the above geomorphic characterization of tidal meanders cannot, of course, be considered complete because properties other than planar are to be considered. Topography is first considered. It has been inferred [*Rinaldo et al.*, 1999a] that topographic gradients are less significant in tidal environments than in hillslope and fluvial geomorphology, owing to the different dynamic implications. In fact, while slopes (and thus gravity) command basin-scale transport, tidal flows are driven mostly by free surface gradients that are weakly dependent on topography. Nevertheless, topographic curvatures can be suitably used to single out the channelized portion of the tidal environments [*Fagherazzi et al.*, 1999a]. Moreover, the bottom profile of tidal channels is usually characterized by an upward concavity which increases with channel convergence [*Lanzoni and Seminara*, 2002]. As a consequence, bottom slope, which may attain relatively high values in the landward reaches, tends to decrease progressively as one moves seaward, thus implying that the flow depth is likely to increase at a rate smaller than the width.

[41] Here we show the results of our survey of width-to-depth ratios $\beta = 2B/D$ in meandering tidal channels and creeks [e.g., *Leopold et al.*, 1993]. Figure 11 shows, for a large sample of channels within the Lagoon of Venice, plots of channel depth D versus width $2B$. The data are derived

from digitized maps for the large channels (say, $B > 10$ m), and result from a direct survey in the test area shown in the inset of Figure 1 for the smaller ones. It should be pointed out that the depth D is computed differently depending on the setup. When small channels flanked by flats placed about the mean sea level are considered, the depth D has been measured relative to the bank-full elevation. This proves accurate and fast, because one does not need to survey exactly the elevation of the bottom. From a dynamic viewpoint, this gives a good estimate of the bank-full cross section, differences with the depth from m.s.l. being of a few tens of centimeters at most. For larger channels extracted from DTMs, where elevations are properly georeferenced, it is expedient (and meaningful from a dynamic viewpoint) to compute depths D from m.s.l.

[42] The plot in Figure 11 shows clear differences in β values. Although important fluctuations occur, salt marsh creeks and tidal flat channels are seen to respond to different erosional processes resulting in different incisions. In salt marshes, the ratio β lies consistently in the range 5-7, quite differently from the values typically observed in meandering rivers (usually $8 < \beta < 48$ [e.g., *Millar*, 2000]). In tidal flats, less incised, river-like patterns are observed ($8 < \beta < 50$). Therefore salt marsh creeks, where the role of vegetation and of cohesive properties of the sediment are likely to strongly affect the erosional processes, tend to be more deeply incised than their fluvial counterparts. On the contrary, the larger channels developing in tidal flats, where vegetation is less likely to play a major role (though submerged Zostera marina bottom fields may be affecting the relevant erosional and accretion processes) and the role of sediment cohesion could be less crucial owing to generally increasing sand fractions, are more similar to fluvial landforms. Thus it is significant that certain regularities are observed in the planar properties though facing such different imprintings of the relevant erosional processes. This also awaits proper theoretical interpretation.

4. Conclusions

[43] We have studied several features of tidal meanders observed in different coastal wetlands. Our main conclusions can be summarized as follows.

1. Substantial differences with fluvial morphologies are observed. In particular, the observations emphasize the role of strong spatial gradients of characteristic geometric features, chiefly wavelength and width, that respond to gradients in landforming discharges. Remarkably, as the dominant discharge markedly increases seaward along a tidal channel, its width adjusts to an exponential growth, whose rate constant is site-specific. Fluctuations are observed but they cannot becloud a clear exponential trend.

2. Spectral models of the parameterized curves describing the spatial patterns of the centerline of meandering channels, in particular of the spatial evolution of local curvature, have been analyzed. Earlier models from fluvial observations and theory prove inadequate in the tidal case owing to a strong presence of even modes, in particular the second one, omitted in the description of river meanders.

3. As the meanders evolve, the (appropriate) meander wavelengths, radii of curvature and width vary by orders of magnitude (say, we recorded widths growing from a few meters to 200 m within a few km alongstream), thus rendering the meandering forms strongly non stationary. Remarkably, however, the ratio of local width to local radius of curvature fluctuates about rather constant values quite different from those observed in meandering rivers. This and other results obtained, i.e., that in both fluvial and tidal environments the ratio of meander length to meander width remains roughly constant, seem to imply that the adjustment of meander morphology to varying dominant discharges is local and does not entail significant transition zones, with many a dynamic implication.

4. Width-to-depth ratios, which bear strong implications on the erosional and migration mechanisms that originate and develop the meanders, vary substantially depending on location and conditions, thus supporting the significance of the observation of certain planar regularities independent of tidal, vegetational, hydrodynamic and sedimentational conditions.

[44] **Acknowledgments.** Funding from 2001 MURST 40% *Idrodinamica e Morfodinamica a Marea* (A. Rinaldo co-ordinator), from CORILA (Consorzio per la Gestione del Centro di Coordinamento delle Attivita' di Ricerca inerenti il Sistema Lagunare di Venezia) (Research Program 2000–2004, Linea 3.2 *Idrodinamica e Morfodinamica and Linea 3.7 Modelli Previsionali*) and by ASI 2001 *Telerilevamento delle reti a marea* (M. Marani coordinator) is gratefully acknowledged.

References

Banavar, J. R., A. Maritan, and A. Rinaldo, Topology of the fittest network, *Phys. Rev. Lett.*, *84*(20), 4745–4748, 2000.

Barwis, J. H., Sedimentology of some South Carolina tidal-creek point bars, and a comparison with their fluvial counterpart, in *Fluvial Sedimentology*, edited by A. D. Miall, *Can. Soc. Petrol. Geol. Mem.*, *5*, 129–160, 1978.

Blondeaux, P., and G. Seminara, A unified bar-bend theory of river meanders, *J. Fluid Mech.*, *157*, 449–470, 1985.

Boon, J. D., Tidal discharge asymmetry in a salt marsh drainage system, *Limnol. Oceanogr.*, *20*, 71–80, 1975.

Boon, J. D., and R. J. Byrne, On basin hypsometry and the morphodynamic response of coastal inlet systems, *Mar. Geol.*, *40*, 27–48, 1981.

Dalrymple, R. W., and R. N. Rhodes, Estuarine dunes and bars, in *Geomorphology and Sedimentology of Estuaries*, edited by G. M. E. Perillo, 359–422, Elsevier Sci., New York, 1995.

Day, J. W., J. Rybczyk, F. Scarton, A. Rismondo, D. Are, and G. Cecconi, Site accretionary dynamics, sea-level rise and the survival of wetlands in Venice lagoon: A field and modelling approach, *Estuarine Coastal Shelf Sci.*, *49*, 607–628, 1999.

Fagherazzi, S., A. Bortoluzzi, W. E. Dietrich, A. Adami, S. Lanzoni, M. Marani, and A. Rinaldo, Tidal networks, 1, Automatic network extraction and preliminary scaling features from digital terrain maps, *Water Resour. Res.*, *35*(12), 3891–3904, 1999a.

Fagherazzi, S., S. Lanzoni, M. Marani, and A. Rinaldo, Sulle reti a marea della Laguna di Venezia, Atti dell'Istituto Veneto di Scienze Lettere ed Arti, *Classe Sci. Fis. Mat. Nat.*, *161*, 19–92, 1999b.

Friedrichs, C. T., Stability, shear stress and equilibrium cross-sectional geometry of sheltered tidal channels, *J. Coastal Res.*, *4*, 1062–1074, 1995.

Friedrichs, C. T., and O. S. Aubrey, Nonlinear tidal distortion in shallow well-mixed estuaries: A synthesis, *Estuarine Coastal Shelf Sci.*, *27*, 521–545, 1988.

Friedrichs, C. T., and O. S. Madsen, Nonlinear diffusion on the tidal signal in frictionally dominated embayments, *J. Geophys. Res.*, *97*, 5637–5650, 1992.

Howard, A. D., Modeling channel migration and floodplain sedimentation in meandering streams, in *Lowland Floodplain Rivers: Geomorphological Perspecteves*, edited by P. A. Carling and G. E. Petts, pp. 1–41, John Wiley, New York, 1992.

Howard, A. D., Modeling channel evolution and floodplain morphology, in *Floodplain Processes*, edited by M. G. Anderson, D. E. Walling, and P. Bates, pp. 15–62, John Wiley, New York, 1996.

Ikeda, I., G. Parker, and K. Sawai, Bend theory of river meanders, part I, Linear development, *J. Fluid Mech.*, *112*, 363–377, 1981.

Kinoshita, R., An investigation of channel deformation of the Ishikari River, technical report, 139 pp., Nat. Resour. Div., Minist. of Sci. and Technol. of Jpn., Tokyo, 1961.

Langhaar, H. L., *Dimensional Analysis and Theory of Models*, Chapman and Hall, New York, 1951.

Lanzoni, S., and G. Seminara, On tide propagation in convergent estuaries, *J. Geophys. Res.*, *103*, 30,793–30,812, 1998.

Lanzoni, S., and G. Seminara, Long-term evolution and morphodynamic equilibrium of tidal channels, *J. Geophys. Res.*, *107*(C1), 3001, doi:10.1029/2000JC000468, 2002.

Leopold, L. B., and M. G. Wolman, River channel pattern: Braided, meandering and straight, *U. S. Geol. Surv. Prof. Pap.*, *282-B*, 1957.

Leopold, L. B., M. G. Wolman, and J. P. Miller, *Fluvial Processes in Geomorphology*, W. H. Freeman, New York, 1964.

Leopold, L. B., J. N. Collins, and L. M. Collins, Hydrology of some tidal channels in estuarine marshlands near San Francisco, *Catena*, *20*, 469–493, 1993.

Lohani, B., and D. C. Mason, Extraction of tidal channel networks from LiDAR data, paper presented at Fourth International Airborne Remote Sensing Conference, NASA, Ottawa, Ontario, Canada, June 1999.

Millar, R. G., Influence of bank vegetation on alluvial chennel patterns, *Water Res. Resour.*, *36*(4), 1109–1118, 2000.

Orson, R., R. Warren, and W. Niering, Development of a tidal marsh in a New England river valley, *Estuaries*, *10*, 20–27, 1987.

Parker, G., K. Sawai, and S. Ikeda, Bend theory of river meanders, part 2, Nonlinear deformation of finite-amplitudes, *J. Fluid Mech.*, *115*, 303–314, 1982.

Pestrong, R., The development of drainage patterns on tidal marshes, *Stanford Univ. Publ. Geol. Sci. Tech. Rep. 10*, Stanford Univ., Stanford, Calif., 1965.

Pethick, J. S., Velocity surges and asimmetry in tidal channels, *Estuarine Coastal Mar. Sci.*, *11*, 331–345, 1980.

Redfield, A. C., Development of a New England salt marsh, *Ecol. Monogr.*, *24*(2), 201–237, 1972.

Rinaldo, A., S. Fagherazzi, S. Lanzoni, M. Marani, and W. E. Dietrich, Tidal networks, 2, Watershed delineation and comparative network morphology, *Water Resour. Res.*, *35*(12), 3905–3917, 1999a.

Rinaldo, A., S. Fagherazzi, S. Lanzoni, M. Marani, and W. E. Dietrich, Tidal networks, 3, Landscape-forming discharges and studies in empirical geomorphic relationships, *Water Resour. Res.*, *35*(12), 3919–3929, 1999b.

Rodriguez-Iturbe, I., and A. Rinaldo, *Fractal River Basins: Chance and Self-Organization*, Cambridge Univ. Press, New York, 1997.

Saccardo, A., Il telerilevamento delle reti a marea: Analisi della morfologia, doctoral thesis, Univ. of Padova, Padova, Italy, 1999.

Seminara, G., G. Zolezzi, M. Tubino, and D. Zardi, Downstream and upstream influence on river meandering, part two, Planimetric development, *J. Fluid Mech.*, *438*, 213–230, 2001.

Sinnock, S., and A. R. Rao, A heuristic method for meaurement and characterization of river meander wavelength, *Water Resour. Res.*, *20*(10), 1443–1452, 1984.

Solari, L., G. Seminara, S. Lanzoni, M. Marani, and A. Rinaldo, Sand bars in tidal channels, part two, Tidal meanders, *J. Fluid Mech.*, *451*, 203–238, 2002.

Speer, P. E., and D. G. Aubrey, A Study of non-linear tidal propagation in shallow inlet/estuarine systems, part II, Theory, *Estuarine Coastal Shelf Sci.*, *21*, 207–224, 1985.

Steel, T. J., and K. Pye, The development of salt marsh tidal creek networks: Evidence from the UK, paper presented at Canadian Coastal Conference 1997, Can. Coastal Sci. and Eng. Assoc., Guelph, Ontario, 1997.

Zandolin, D., Analisi Morfologica delle Reti a Marea, doctoral thesis, Univ. di Padova, Padova, Italy, 1999.

S. Lanzoni, M. Marani, A. Rinaldo, and D. Zandolin, Dipartimento di Ingegneria Idraulica, Marittima e Geotecnica, Universitá di Padova, via Loredan 20, I-35131 Padova, Italy. (lanzo@idra.unipd.it; marani@idra.unipd.it; rinaldo@idra.unipd.it; zandolin@idra.unipd.it)

G. Seminara, Dipartimento di Ingegneria Ambientale, Universitá di Genova, via Montallegro, 1, 16122 Genova, Italy. (sem@idra.unige.it)